



LAWRENCE  
LIVERMORE  
NATIONAL  
LABORATORY

LLNL-JRNL-416293

# Electron-ion thermal equilibration after spherical shock collapse

J. R. Rygg, J. A. Frenje, C. K. Li, F. H. Seguin, R.  
D. Petrasso, D. D. Meyerhofer, C. Stoeckl

August 28, 2009

Physical Review E

## **Disclaimer**

---

This document was prepared as an account of work sponsored by an agency of the United States government. Neither the United States government nor Lawrence Livermore National Security, LLC, nor any of their employees makes any warranty, expressed or implied, or assumes any legal liability or responsibility for the accuracy, completeness, or usefulness of any information, apparatus, product, or process disclosed, or represents that its use would not infringe privately owned rights. Reference herein to any specific commercial product, process, or service by trade name, trademark, manufacturer, or otherwise does not necessarily constitute or imply its endorsement, recommendation, or favoring by the United States government or Lawrence Livermore National Security, LLC. The views and opinions of authors expressed herein do not necessarily state or reflect those of the United States government or Lawrence Livermore National Security, LLC, and shall not be used for advertising or product endorsement purposes.

# Electron-ion thermal equilibration after spherical shock collapse

J. R. Rygg<sup>\*</sup>, J. A. Frenje, C. K. Li, F. H. Séguin, and R. D. Petrasso<sup>†</sup>

*Plasma Science and Fusion Center, Massachusetts Institute of Technology, Cambridge, Massachusetts 02139*

D. D. Meyerhofer<sup>‡</sup> and C. Stoeckl

*Laboratory for Laser Energetics, University of Rochester, Rochester, New York 14623*

(Draft July 24, 2009, submitted to Phys. Rev. E)

A comprehensive set of dual nuclear product observations provides a snapshot of imploding inertial confinement fusion capsules at the time of shock collapse, shortly before the final stages of compression. The collapse of strong convergent shocks at the center of spherical capsules filled with  $D_2$  and  $^3He$  gas induces D-D and D- $^3He$  nuclear production. Temporal and spectral diagnostics of products from both reactions are used to measure shock timing, temperature, and capsule areal density. The density and temperature inferred from these measurements are used to estimate the electron-ion thermal coupling, and demonstrate a lower electron-ion relaxation rate for capsules with lower initial gas density.

## I. INTRODUCTION

Converging spherical shocks and electron-ion thermal equilibration are basic physical processes [1] of fundamental importance for the design of high gain implosions in inertial confinement fusion (ICF) [2-4]. Strong, spherically convergent shocks are formed by the rapid deposition of energy in the form of lasers (direct-drive) or x rays (indirect-drive) on the surface of a spherical capsule. Current “hot-spot” ICF ignition designs include a sequence of up to four convergent shocks that must be precisely timed to coalesce at the inner shell surface so as to obtain maximal shell compression [5,6], a necessity for high fusion gain. Other ignition designs include the launching of a convergent shock into a

<sup>\*</sup> Now at Lawrence Livermore National Laboratory

<sup>†</sup> Also Visiting Senior Scientist at LLE.

<sup>‡</sup> Also Departments of Mechanical Engineering, and Physics and Astronomy.

compressed fuel assembly [7]. In both cases, ICF implosion design and performance is deeply affected by the speed and heating of convergent shocks through ambient and compressed materials.

Shocks initially deposit thermal energy primarily in the ions, and the ensuing electron-ion thermal equilibration is one of many related transport processes of concern for ICF modelers [3,4]. Recent theoretical [8,9,10] and computational [11,12,13] work have helped to clarify ambiguities in the Landau-Spitzer energy equilibration rate [14,15], which result from ad-hoc cutoffs of logarithmic divergences in the Coulomb collisional rates. Previous experimental and observational investigations of electron-ion thermal relaxation includes the work of Celliers *et al.* [16,17] and Laming *et al.* [18], and new investigations are currently underway [19,20].

This article presents the first results of temporal and spectral measurements of products from two simultaneous nuclear reaction types induced by the central collapse of convergent shocks. Nuclear measurements of some aspects of shock collapse using a single nuclear product have been reported recently [21,22,23]. Observations of these products supply compelling information about the speed and heating of the shocks, and the state of the imploding capsule at the time of shock collapse. In the experiments discussed here this occurs immediately before the onset of the deceleration phase and the final stages of compression. The comprehensive picture of the central shocked gas provided by the dual nuclear reaction measurements is used to evaluate electron-ion thermal equilibration in the plasma after shock collapse.

Section II describes the experimental setup, and Section III, the experimental results. Various plasma parameters of the central shocked gas are derived from the measurements in Section IV. A brief review of electron-ion thermal equilibration after shock heating is outlined in Section V, and is applied to the experimental observations in Section VI. Concluding remarks are presented in Section VII.

## II. EXPERIMENTAL SETUP

Direct-drive spherical capsule implosions were conducted using the OMEGA laser system [24], with 60 beams of ultraviolet (351 nm) light in a 1-ns square pulse, a total energy of 23 kJ, and full single-beam smoothing [25]. The resulting  $1 \times 10^{15}$  W/cm<sup>2</sup> intensity was incident on capsules with diameters between 855 and 875  $\mu\text{m}$ , plastic (CH, density 1.04 g/cm<sup>3</sup>) shell thicknesses ( $\Delta R$ ) of 20, 24, or 27  $\mu\text{m}$ , and a flash coating of 0.1  $\mu\text{m}$  of aluminum. The capsules were filled with an equimolar (by atom) mixture of D<sub>2</sub> and <sup>3</sup>He gas with a total fill pressure of 3.6 or 18 atm at 293 K, corresponding to initial gas mass densities ( $\rho_0$ ) of 0.5 and 2.5 mg/cm<sup>3</sup>, respectively.

Three distinct primary nuclear reactions occur during capsule implosions with D<sub>2</sub> and <sup>3</sup>He fuel:



The neutron (1) and proton (2) branches of the DD reaction have nearly equal probabilities over temperatures of interest. The D<sup>3</sup>He reaction depends much more strongly on temperature due to the doubly-charged <sup>3</sup>He reactant [26]. The mean birth energies of D<sup>3</sup>He and DD protons are 14.7 and 3.0 MeV, respectively.

Nuclear products were observed using the proton and neutron temporal diagnostics (PTD and NTD) [22,27], to measure the D<sup>3</sup>He and DD-n reaction histories; multiple wedge-range-filter proton spectrometers [28], to measure the D<sup>3</sup>He proton yield and spectrum; and a magnet-based charged-particle spectrometer [28], to obtain the first measurements of DD protons emitted at shock-bang time.

The D<sup>3</sup>He reaction rate history shows two distinct times of nuclear production (Fig 1a): “shock-burn” begins shortly after shock collapse, and ends near the beginning of the deceleration of the shell; “compression-burn” lags about 300 ps after shock burn, beginning near the onset of shell deceleration,

and lasting approximately until the stagnation of the imploding shell (Fig. 2). For ordinary  $D_2$ - $^3He$  mixtures, the DD-n reaction rate during the shock burn is below the diagnostic detection threshold.

The shock and compression components can often be distinguished in  $D^3He$  proton spectra (Fig 1b) [21]. The protons emitted during shock-burn experience relatively little downshift ( $\sim 0.4$  MeV) due to the low total capsule areal density ( $\rho R$ ) at that time. The shell continues to compress after shock-burn ends, and by the time of compression-burn the  $\rho R$  has increased enough to downshift  $D^3He$  protons by several MeV.

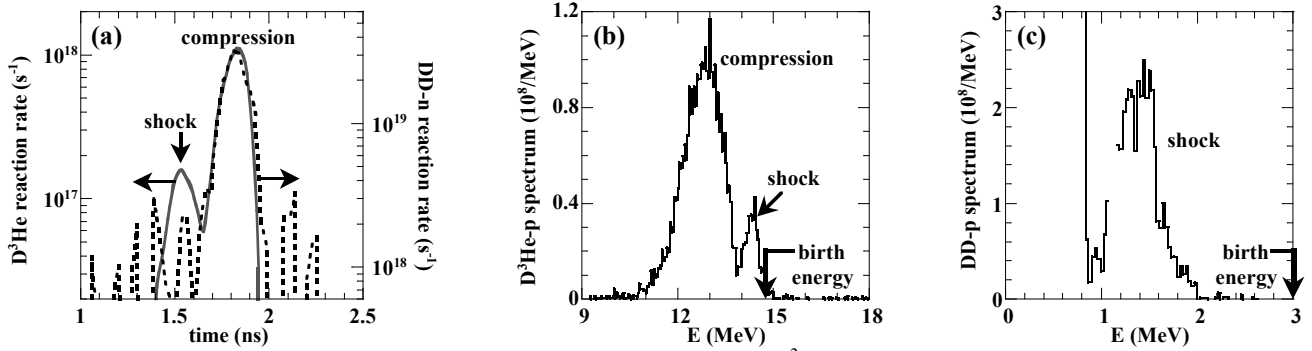


Fig. 1. Representative experimental observations of DD and  $D^3He$  nuclear products emitted at shock- and compression-bang time from an implosion of a 24  $\mu m$ -thick CH capsule shell filled with 2.5  $mg/cm^3$  of  $D_2$ - $^3He$  gas (OMEGA shot 38525). (a)  $D^3He$  (solid) and DD-n (dotted) reaction rate histories. (b)  $D^3He$ -proton spectrum. (c) DD-proton spectrum.

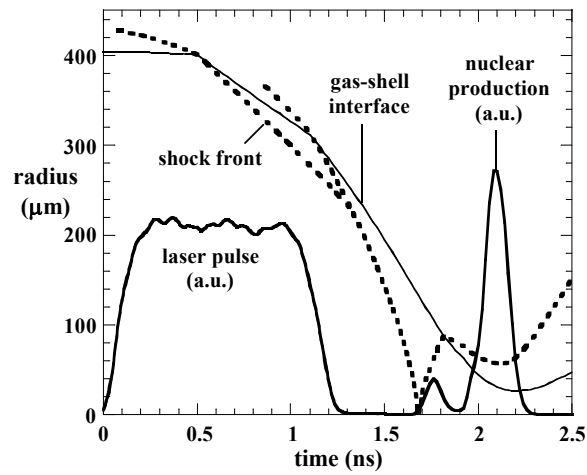


Fig. 2. A representative 1-D simulation shows the  $D^3He$  nuclear reaction rate and trajectories of the gas-shell interface and the converging shock. Collapse of the converging shock induces nuclear “shock-burn” about 300 ps before the compression-burn peak and stagnation of the imploding shell. Reproduced from Ref. [23].

The  $\rho R$  during shock-burn is low enough to allow nascent 3.0 MeV DD protons to escape the capsule (Fig 1c), but the DD protons are ranged out in the capsule during compression-burn due to the higher capsule  $\rho R$  at that time. Measurement of DD protons emitted during shock-burn provides a valuable and sole measurement of the DD shock yield when the reaction rate is below the NTD threshold (as is often the case). Measurement of their downshift provides a double check on the  $\rho R$  at shock-bang time inferred using the  $D^3He$  proton spectra, or the sole measurement in cases where the shock component of the  $D^3He$  proton spectrum cannot be separated from the compression component.

### III. EXPERIMENTAL RESULTS

Measured shock-bang times and  $D^3He$  and DD-p shock yields are shown in Fig. 3 as a function of  $\Delta R$  for implosions of capsules with different  $\rho_0$  (see also Table I). The shock-bang time ( $t_s$ ) is the time of peak  $D^3He$  nuclear production during the shock-burn phase; the shock-burn duration ( $\Delta t_s$ ) is the full temporal width at half the maximum shock-burn production rate; the  $D^3He$  shock yield ( $Y_{D^3He}$ ) includes only the contribution from the higher-energy “shock” component of the  $D^3He$ -proton spectrum, and the DD-p shock yield ( $Y_{DD}$ ) includes only that part of the spectrum above the high-energy cutoff of protons accelerated from the shell [29] (seen at 0.8 MeV in Fig 1c). Fig. 3 plots the mean and the standard deviation of the mean for implosion ensembles of each capsule configuration. Shot-by-shot tables of most of the experimental results are available in Ref. [30].

Experiments show that  $t_s$  is linearly delayed with increasing  $\Delta R$  (Fig. 3a). No difference in  $t_s$  was observed for capsules with different  $\rho_0$ . For capsules with the same  $\Delta R$ , identical shocks should be generated in the shell with identical drive conditions (as is approximately the case here), and the shocks should break into the gas at the same time. Since  $t_s$  is independent of  $\rho_0$ , we conclude that shocks of the same speed are launched into the gas for implosions with the same  $\Delta R$  and drive.

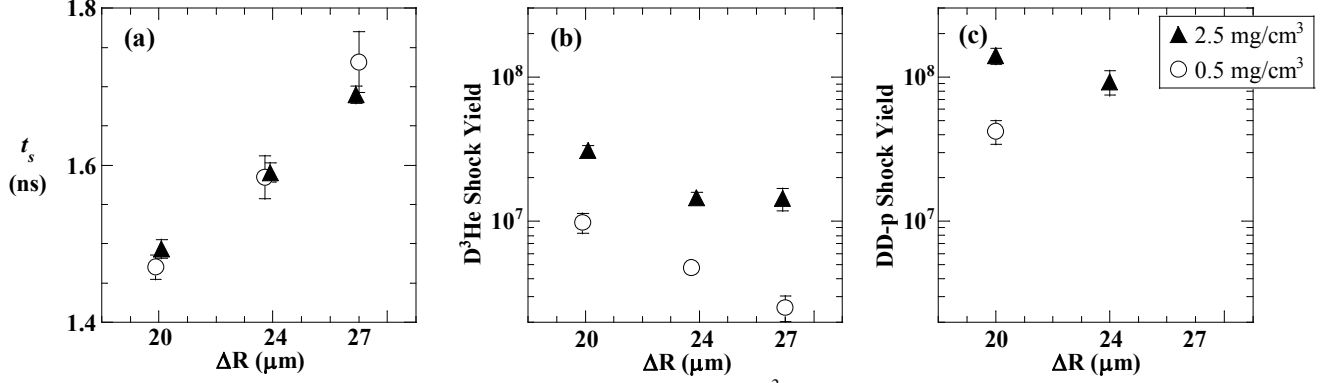


Fig. 3. Experimental observations of (a) shock-bang time, (b)  $D^3He$  shock yield, and (c) DD-p shock yield as a function of capsule shell thickness for ensembles of capsules filled with 2.5 (triangles) or 0.5  $mg/cm^3$  (circles) of  $D^3He$  gas. In some cases, the error bars (representing the standard error of the ensemble mean) is smaller than the marker size.

Table I. Mean and standard deviation of the mean of shock measurements with  $D^3He$  and DD protons for implosion ensembles of different initial gas density ( $\rho_0$ ) and capsule shell thickness ( $\Delta R$ ). Each ensemble consists of  $N$  ( $N_{DD}$ ) implosions with  $D^3He$  (DD-p) measurements. The  $D^3He$  ensemble includes shock-bang time ( $t_s$ ), shock-burn duration ( $\Delta t_s$ ),  $D^3He$  shock yield ( $Y_{D^3He}$ ), shock areal-density ( $\rho R_{s-d^3he}$ ), and inferred gas compression ratio ( $\rho_s/\rho_0$  [ $D^3He$ ]). The remaining quantities are from the DD ensemble, including the DD-p shock yield ( $Y_{DD}$ ), and the shock-burn averaged ion temperature ( $T_{si}$ ).

$\rho_0$ (mg/cc)	$\Delta R$ ( $\mu m$ )	diam. ( $\mu m$ )	$N$ ( $N_{DD}$ )	$t_s$ (ps)	$\Delta t_s$ (ps)	$Y_{D^3He}$ ( $\times 10^7$ )	$Y_{DD}$ ( $\times 10^7$ )	$T_{si}$ (keV)	$\rho R_{s-d^3he}$ (mg/cm <sup>2</sup> )	$\rho R_{s-dd}$ (mg/cm <sup>2</sup> )	$\rho_s/\rho_0$ [ $D^3He$ ]	$\rho_s/\rho_0$ [DD]
0.5	19.9	862	8 (5)	$1470 \pm 16$	$129 \pm 18$	$0.98 \pm 15\%$	$4.2 \pm 10\%$	$7.7 \pm 0.7$	-	$8.3 \pm 0.7$	-	$22 \pm 3$
0.5	23.7	873	6 (0)	$1585 \pm 27$	$129 \pm 11$	$0.48 \pm 9\%$	-	-	$9.8 \pm 0.4$	-	$17 \pm 1$	-
0.5	27.0	873	4 (0)	$1731 \pm 39$	$122 \pm 30$	$0.25 \pm 20\%$	-	-	$12.0 \pm 0.9$	-	$17 \pm 2$	-
2.5	20.1	863	8 (3)	$1493 \pm 12$	$145 \pm 13$	$3.09 \pm 7\%$	$14.1 \pm 13\%$	$5.8 \pm 0.3$	$8.2 \pm 1.0$	$9.3 \pm 0.6$	$18 \pm 3$	$23 \pm 3$
2.5	23.9	865	9 (3)	$1591 \pm 12$	$137 \pm 10$	$1.45 \pm 9\%$	$9.2 \pm 20\%$	$5.4 \pm 0.4$	$9.1 \pm 0.7$	$10.0 \pm 0.7$	$14 \pm 1$	$16 \pm 2$
2.5	26.9	873	6 (2)	$1690 \pm 11$	$146 \pm 10$	$1.44 \pm 18\%$	-	-	$9.4 \pm 1.2$	$11.1 \pm 1.0$	$14 \pm 2$	$15 \pm 2$

Both  $D^3He$  and DD shock yields were observed to decrease for implosions of targets with thicker shells and lower  $\rho_0$ . However, the expected yield reduction – due only to the density dependence of the nuclear fusion rate – from high to low  $\rho_0$  is 25, a much higher value than the observed reduction of between 3 and 5. This indicates that lower fill density also results in reduced thermal coupling between ions and electrons (see Section V), so that the ion temperature, and consequently the nuclear fusion rate, remains high.



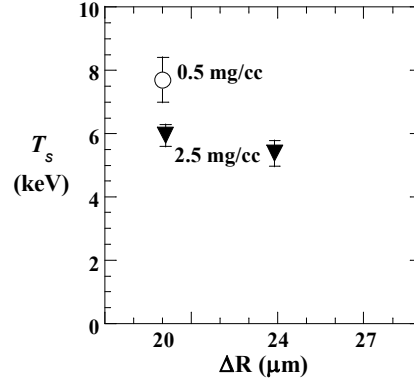


Fig. 4. Shock-burn averaged ion temperature vs  $\Delta R$  for two different  $\rho_0$ , calculated using the ratio of measured DD-p to  $\text{D}^3\text{He}$  shock yields. Although shocked to the same initial ion temperature at a given shell thickness, thermal coupling with electrons is weaker in the low  $\rho_0$  implosions.

The average ion temperature [31] at shock-bang time  $T_{si}$  can be inferred using the measured yields of the two different nuclear reactions, based on the ratio of their respective thermal reactivities [26]. This method has previously been used to infer ion temperature during the compression burn by Li *et al.* [32] and Frenje *et al.* [22]. Fig. 4 plots the  $T_{si}$  inferred by this method, showing higher  $T_{si}$  for low  $\rho_0$  implosions.

The compression of the capsule at shock-bang time can be quantified by the shock-burn averaged [31] areal density,  $\rho R_s$ . The areal density at shock time is of particular concern in ICF because the value of  $\rho R_s$  sets the initial condition for the final capsule compression to the stagnation  $\rho R$ , which in turn is a fundamental metric of capsule assembly, and is essential for ignition and efficient nuclear burn [2-4]. Experimentally,  $\rho R_s$  is inferred from the measured mean energy downshift from the birth energy of DD protons ( $\rho R_{s,DD}$ ) or  $\text{D}^3\text{He}$  protons in the shock line ( $\rho R_{s,D^3He}$ ), using a theoretical formalism to relate their energy loss to plasma parameters [28,33]. The inferred  $\rho R_s$  value is insensitive to the exact parameter values assumed, particularly when using the downshift of 14.7 MeV  $\text{D}^3\text{He}$  protons; a CH plasma density of  $3 \text{ g/cm}^3$ , and temperature of 0.3 keV was used to derive the quoted  $\rho R_s$  values.

Substantial agreement is observed between  $\rho R_s$  inferred from spectral results obtained using both DD and  $\text{D}^3\text{He}$  protons, as seen in Fig 5 and Table I. Implosions with increasing  $\Delta R$  show an increase in  $\rho R_s$  due to the larger remaining shell mass at shock time. On the basis of physical principles, the

contribution of the shell to the areal density  $\rho R_{s,shell}$  should be only weakly dependent on the initial gas density  $\rho_0$ , since the trajectory of the high-density shell will be almost unaffected by the fill gas until the shell starts to decelerate several hundred picoseconds after shock-bang time. As we will see in Section IV,  $\rho R_s$  is dominated by the shell contribution, and should also be weakly dependent on  $\rho_0$ . The data shown in Fig 5 and Table I are consistent with this viewpoint.

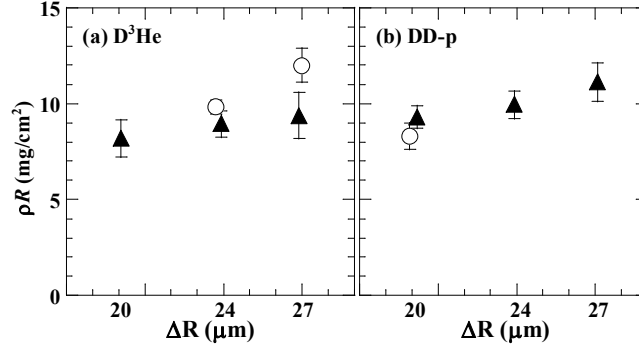


Fig. 5. Shock-burn averaged areal density  $\rho R_s$  vs.  $\Delta R$  for  $D^3He$  fills of  $2.5 \text{ mg/cm}^3$  (triangles) and  $0.5 \text{ mg/cm}^3$  (circles).  $\rho R_s$  is inferred from the downshift of nascent (a) 14.7 MeV  $D^3He$  protons and (b) 3 MeV DD-protons from their birth energy. Markers show mean and standard error.

#### IV. CHARACTERIZATION OF THE SHOCKED GAS

Theoretical analysis suggests that converging shocks are weakly unstable to initial asymmetries [34]; however, experiments have demonstrated that the nuclear observables are highly robust to drive asymmetries [23], and that the growth of asymmetries due to hydrodynamic instabilities is insufficient to mix the shell with the fill gas at during the shock-burn [35]. Thus, the behavior of the imploding capsule at the time of shock-burn can be well described by a 1-dimensional, spherically-symmetric model.

The shock-burn averaged plasma density  $\rho_s$  can be estimated from our measurements of the shock-burn averaged total areal density  $\rho R_s$ . Assuming thin shells and a spherically symmetric model of the implosion and invoking mass conservation gives

$$\frac{\rho_s}{\rho_0} = \left( \frac{\rho R_s}{\rho R_{0,gas} + f \rho R_{0,shell}} \right)^{3/2}, \quad (4)$$

where  $\rho R_{0,gas}$  and  $\rho R_{0,shell}$  are the initial areal densities of the gas and the shell before the implosion, and  $f$  is the fraction of the initial shell mass remaining after ablation of the outer shell by the drive laser intensity. The mass ablation rate  $dm/dt$  is [3,4]

$$\frac{dm}{dt} (g / cm^2 / s) = 2.6 \times 10^5 \left( \frac{I_{15}}{\lambda^4} \right)^{1/3}, \quad (5)$$

where  $I_{15}$  is the laser intensity in  $10^{15}$  W/cm<sup>2</sup> and  $\lambda$  is the laser wavelength in microns. For these experiments, about 10  $\mu$ m of the original shell is ablated during the laser pulse, giving a volumetric compression ratio at shock time  $\rho_s/\rho_0$  of 14-23 (see Table I). The inferred compression ratios are apparently equal for implosions with the same  $\Delta R$  but different  $\rho_0$ , which is consistent with the expectation stated in the previous section.

Using these values of the compression ratio, mass conservation can be used to estimate the areal density of the fuel at shock time  $\rho R_{s,gas}$ :

$$\rho R_{s,gas} = \rho R_{0,gas} \left( \frac{\rho_s}{\rho_0} \right)^{2/3}, \quad (6)$$

which gives values of 0.15 mg/cm<sup>2</sup> and 0.6-0.8 mg/cm<sup>2</sup>, contributing 1-2% and 6-9% of the total  $\rho R_s$  for low and high  $\rho_0$ , respectively.

Simultaneous knowledge of the gas composition, density, and temperature allows some basic plasma parameters to be computed. For definiteness, the following discussion is restricted to the case of the  $\Delta R = 20$   $\mu$ m ensemble with high (low)  $\rho_0$ . The DD-inferred compression ratio,  $\sim 22$ , is the same for all  $\rho_0$ , but is slightly higher than the D<sup>3</sup>He inferred compression ratio, 18, for high  $\rho_0$ . The average of these methods gives a compression ratio  $\rho_s/\rho_0 = 20$ , which will be used for both ensembles. In this case, at shock-bang time, the mass density  $\rho_s = 50$  (10) mg/cm<sup>3</sup>, the electron density  $n_e = 18$  (3.6)  $\times 10^{21}$  cm<sup>-3</sup>, and the Fermi energy  $E_f = \hbar^2 (3\pi^2 n_e)^{2/3} / 2m_e = 2.5$  (0.86) eV, where  $\hbar$  is the reduced Planck constant, and  $m_e$  is the electron mass.

As will be shown in Section V, the electron temperature  $T_e$  averaged over shock-burn is 2.0 (0.73) keV, which establishes that the electrons can be treated as non-degenerate: the electron degeneracy parameter  $\Theta = T_e/E_f = 800$  (850)  $\gg 1$ . Both the electron and ion temperatures are much higher than the final ionization energies of atomic D and  $^3\text{He}$  (D: 13.6 eV,  $^3\text{He}$ : 54.4 eV), so the gas is a fully ionized plasma.

The pressure in a non-degenerate fully ionized plasma is given by the ideal kinetic gas pressure,  $P = (n_e T_e + n_i T_i) = 17$  (3.4) TPa. As temperatures in this article are expressed in energy units, Boltzmann's constant  $k_B$  has been suppressed. The plasma parameter, related to the number of particles in a Debye sphere, is  $(\epsilon_0 T_e / e^2 n_e)^{3/2} = 1900$  (950)  $\gg 1$ .  $\epsilon_0$  is the permittivity of free space and  $e$  is the fundamental charge.

The Coulomb logarithm,  $\ln \Lambda = \ln(b_{\max}/b_{\min})$ , is important for many plasma transport properties, including thermal equilibration, but there is some variation in the precise impact parameter cutoffs  $b_{\max}$  and  $b_{\min}$  [13,15]. Here, we use the value of  $\ln \Lambda$  given by Ref. [10] in the non-degenerate limit,

$$\ln \Lambda = \ln \left( \frac{T_e}{\hbar \omega_{pe}} \right) - 1.8283, \quad (7)$$

where  $\omega_{pe} = (e^2 n_e / \epsilon_0 m_e)^{1/2}$  is the electron plasma frequency. For the gas at shock time, Eq. (7) gives  $\ln \Lambda = 6.2$  (6.0).

It should be emphasized that this characterization of the shocked gas completely ignores many attributes of this highly dynamic and non-uniform system, including steep temperature and density gradients, non-thermal velocity components, and rapid temporal evolution. However, describing the plasma in this “shock-averaged” manner [31] offers valuable information about the state of the imploding capsule immediately before the onset of deceleration phase, both as an initial condition of, and in contrast to the compression burn. In addition, comparison of the shock states with different  $\rho_0$  allows the value of the electron-ion thermal equilibration rate to be inferred experimentally.

## V. THERMAL EQUILIBRATION

If a strong, non-radiating shock propagating at speed  $u_s$  through a uniform ideal gas is sufficiently strong to fully ionize the gas (as is the case here), it will distribute thermal energy among the electron and ion species according to their masses  $m_j$ , such that the immediate post-shock temperatures  $T_{0j}$  are (e.g., see Ref. [36]):

$$T_{0j} = \frac{3}{16} m_j u_s^2, \quad (8)$$

where  $j = e, i$  for electrons and ions.

The large mass difference between the ions and electrons ( $\sim 4600$  for the equimolar D-<sup>3</sup>He mixture considered here) endows each species with widely different initial temperatures, but otherwise depends only on the shock speed. The electron and ion temperatures ( $T_e$  and  $T_i$ ) relax over time to a final equilibrium temperature  $T_f$  as energy is exchanged through Coulomb collisions. In the absence of thermal conduction, the sum of  $T_e$  and  $T_i$  is constrained by energy conservation according to their relative heat capacities,

$$T_i + ZT_e = T_{0i} + ZT_{0e} = (1 + Z)T_f, \quad (9)$$

where  $Z = 1.5$  is the average ion atomic number. Note that  $ZT_{0e} \ll T_{0i}$ .

The rate of temperature equilibration is usually expressed as the ratio of the temperature difference over a characteristic time [1, 15],

$$\frac{dT_e}{dt} = \frac{T_i - T_e}{\tau_{ei}}, \quad (10)$$

where  $\tau_{ei}$  is the electron-ion thermal equilibration time constant [37,38] and is temperature dependent,

$$\frac{\tau_{ei}}{\tau_f} = \left( \frac{T_e}{T_f} \right)^{3/2}. \quad (11)$$

$\tau_f$  is the density-dependent coupling time constant at the equilibrium temperature [4,13,15],

$$\tau_f = \frac{3}{8\sqrt{2\pi}} \left( \frac{4\pi\epsilon_0}{e^2} \right)^2 \frac{m_i^2}{Z^2 m_e^{1/2}} \frac{T_f^{3/2}}{\rho \ln \Lambda_f}. \quad (12)$$

Here,  $\rho$  is the mass density and  $\ln \Lambda_f$  is the Coulomb logarithm given by Eq. (7) with  $T_e \rightarrow T_f$ . The small logarithmic dependence of  $\ln \Lambda_f$  on temperature has been neglected in Eq. (11).

Using Eqs. (9) and (11), Eq. (10) becomes

$$\frac{dT_e}{dt} = \frac{(1+Z)T_f}{\tau_f} \frac{1-T_e/T_f}{(T_e/T_f)^{3/2}}. \quad (13)$$

Replacing  $T_e/T_f \rightarrow T$  and  $t/\tau_f \rightarrow t$ , the integral representation is:

$$(1+Z) \int dt = \int \frac{T^{3/2} dT}{1-T}, \quad (14)$$

which is analytically integrable,

$$(1+Z)t = 2 \tanh^{-1}[\sqrt{T}] - \frac{2}{3} \sqrt{T} (T+3). \quad (15)$$

Fig. 6 is a plot of this relation for  $Z = 1.5$ .

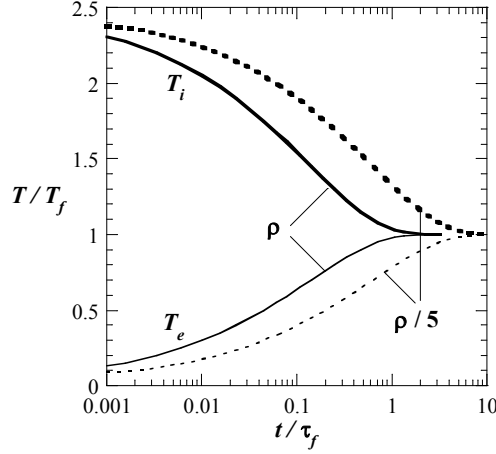


Fig. 6. Electron-ion thermal equilibration for  $Z = 1.5$ . Ion (bold lines) and electron (thin lines) temperatures approach to within a few % of their equilibrium value by time  $\tau_f$ . Thermal relaxation for plasmas with  $1/5$  of the reference mass density takes approximately 5 times as long (dotted lines).

## VI. MEASURING THERMAL EQUILIBRATION

The initial ion temperature  $T_{0i}$  imparted by the shock in Eq. (8) depends only on  $m_i$  and  $u_s$ . The experimental results reported above are consistent with the independence of  $u_s$  on the initial gas density  $\rho_0$ . Since the same gas composition was used for all experiments, this implies that the converging shocks launched into capsules with different  $\rho_0$  nonetheless are heated to the same  $T_{0i}$ . These situations have coupling rates different by a known factor, since the equilibrium time constant  $\tau$  depends on  $\rho_s$ .

$T_{0i}$  can be estimated using the finite difference form of Eq. (10),

$$\frac{\Delta T_e}{\Delta t} = \frac{T_i - T_e}{\tau_{ei}}. \quad (16)$$

Using Eq. (9) and assuming  $T_{0e}$  is negligible,  $\Delta T_e = T_e = (T_{0i} - T_i)/Z$ , and

$$\frac{T_{0i} - T_i}{\Delta t} = \frac{(1 + Z)T_i - T_{0i}}{\tau_{ei}}. \quad (17)$$

If  $T_i$  reaches the measured shock-burn-averaged ion temperature  $T_{si}$  after  $\Delta t$  equal to half the burn duration  $\Delta t_s$ , then all quantities are known except for  $T_{0i}$  and  $\tau_{ei}$ . These values have a known relationship for high and low  $\rho_0$ , so the two sets of measurements are combined to solve for  $T_{0i}$ . Using indices 1 and 2 for high and low  $\rho_0$ , we obtain:

$$\frac{\Delta t_{s2}}{\Delta t_{s1}} \frac{T_{0i} - T_{s1}}{T_{0i} - T_{s2}} = \frac{\tau_{f2}}{\tau_{f1}} \frac{(1+Z)T_{s1} - T_{0i}}{(1+Z)T_{s2} - T_{0i}}. \quad (18)$$

From Table 1,  $\Delta t_{s2}/\Delta t_{s1} = 0.89$ , and from Eq. (12),  $\tau_{f2}/\tau_{f1} = 4.5$ . Defining  $k = (\Delta t_{s2}/\Delta t_{s1}) \times (\tau_{f1}/\tau_{f2})$ , and expanding gives a quadratic equation for  $T_{0i}$ :

$$k(T_{0i} - T_1)[(1+Z)T_2 - T_{0i}] = (T_{0i} - T_2)[(1+Z)T_1 - T_{0i}], \quad (19)$$

with coefficients:

$$\begin{aligned} a &= (1 - k), \\ b &= k[(1+Z)T_2 + T_1] - (1+Z)T_1 - T_2, \\ c &= (1 - k)(1+Z)T_1T_2. \end{aligned} \quad (20)$$

Using the values from Table 1, solutions for  $T_{0i}$  at 12.7 and 8.8 keV are obtained. The 12.7 keV solution is rejected as too high compared to observations of  $T_{si}$  [39]. The 8.8 keV solution corresponds to an equilibrium temperature  $T_f = 3.5$  keV. This is substantially lower than our measured  $T_{si}$  of 5.8 (7.7) keV for high (low)  $\rho_0$ , indicating that both implosion types are far from thermal equilibrium during the shock burn.

With this shock-burn averaged estimate of  $T_{0i}$ , Eq. (9) and the measurements of  $T_{si}$  are used to estimate the shock-burn averaged electron temperature, giving  $T_{se} = 2.0$  (0.73) keV, as stated in Section IV. In that section we also estimated the plasma density  $\rho_s$ , which with  $T_{se}$  can be used to calculate the shock-burn averaged  $\tau_{ei}$  by Eqs. (11) and (12), giving characteristic times of 410 (470) ps [40]. These coupling times are longer than the shock burn duration, indicating that both implosion types have a large temperature difference at the end of the shock burn.

The initially surprising similarity of the characteristic time constants for high and low  $\rho_s$  can be explained by considering that the electrons in the high  $\rho_s$  implosion have already absorbed much more thermal energy, thereby increasing the time constant as it takes more collisions to heat them further. More illustrative of the difference in the equilibration rates are the ion temperature relaxation curves according to Eq. (15), plotted in Fig. 7 for high and low  $\rho_s$  from an initial temperature  $T_{0i} = 8.8$  keV.



From the figure, it is evident that the slopes of the two relaxation curves are similar except for very near  $t = 0$ , when the high  $\rho_s$  plasma undergoes rapid equilibration.

Also shown in Fig. 7 are the measured burn duration and burn-averaged ion temperature  $T_{si}$  for implosions with high and low  $\rho_0$ . The temperature relaxation curves calculated in the simple model are consistent with the average ion temperature inferred from nuclear yield measurements. However, it should again be noted that the central gas during the shock burn is far from the uniform plasma assumed here, as the shock reflected after collapse will heat the fuel to different initial temperatures at different times as it propagates outwards towards the incoming shell.

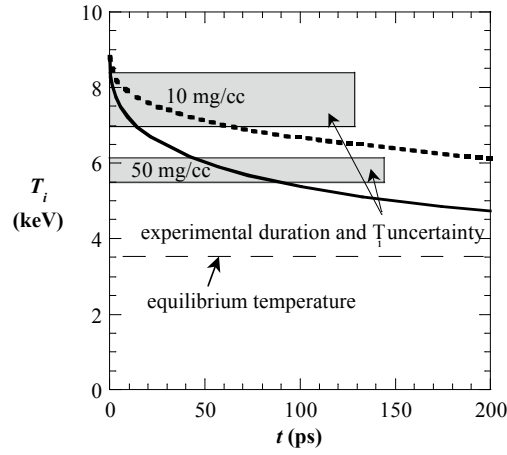


Fig. 7. Ion temperature relaxation for  $D^3He$  plasmas of density  $\rho_s = 50$  (solid) and  $10$  (dotted)  $mg/cm^3$ . The curves represent the temperature equilibration starting at an initial ion temperature  $T_{0i} = 8.8$  keV (corresponding to  $T_f = 3.5$  keV). The width of the grey boxes represents the average measured shock-burn duration, and the height represents the 1-sigma confidence interval of the experimental shock-burn-averaged ion temperature,  $T_{si}$ . Compression-burn overwhelms the shock-burn dynamics starting  $\sim 200$  ps after shock collapse.

## VII. CONCLUSIONS

In summary, nuclear production induced by the collapse of strong, spherically convergent shocks was observed using temporal and spectral measurements of products from two distinct, simultaneous nuclear reaction processes. These dual nuclear shock burn measurements, hitherto unavailable, create a comprehensive description of the state of the implosion immediately after shock collapse time – with gas ion temperatures, gas electron densities, and total areal densities at shock-bang time near 6 keV,  $10^{22}$  e<sup>-</sup>/cm<sup>3</sup> and 10 mg/cm<sup>2</sup>, respectively.

The extensive information provided by these shock burn measurements demonstrate that the ions and electrons are far from thermal equilibrium at the end of the shock burn – particularly so for plasmas of lower density. Ion temperature relaxation curves are calculated with a theoretical thermal equilibration model [10], using plasma parameters inferred from shock-yield-averaged measurements. These calculated ion temperature curves – which assume the plasma to be otherwise static and uniform – are consistent with the observed temperatures, despite the dynamic and highly non-uniform plasma state.

Future experiments could explore thermal equilibration in denser plasmas using simple modifications of the methods described herein. For example, the shell could be filled to larger initial density, either with cryogenically cooled gas, or alternatively with  $^3\text{He}$ -wetted, deuterated-plastic foam. Plasmas at much higher areal densities can be investigated with this technique using  $\text{D}^3\text{He}$  protons and DD neutrons if the compression component can be suppressed or significantly delayed, perhaps by using thicker shells, greater energy, or shaped laser pulses. The application of one or more of these modifications would further enhance the e-i thermal coupling and push the investigation of temperature equilibration towards the challenging strongly coupled plasma regime.

## ACKNOWLEDGEMENTS

The authors express their gratitude to the OMEGA engineers and operations crew who supported these experiments. This work was supported in part by the U.S. Department of Energy Office of Inertial Confinement Fusion (Grant No. DE-FG03-03NA00058), and by the Laboratory for Laser Energetics (Subcontract No. 412160-001G) under Cooperative Agreement DE-FC52-92SF19460, University of Rochester, and New York State Energy Research and Development Authority, and performed in part under the auspices of the U.S. Department of Energy by Lawrence Livermore National Laboratory under Contract DE-AC52-07NA27344.

-----

- [1] Ya. B. Zel'dovich and Yu. P. Raizer, *Physics of Shock Waves and High-Temperature Hydrodynamic Phenomena* (Dover Publications, Mineola, New York 2002).
- [2] J. Nuckolls *et al.*, Nature 239, 139 (1972).
- [3] J. D. Lindl, *Inertial Confinement Fusion*, Springer-Verlag, New York (1999).
- [4] S. Atzeni and J. Meyer-Ter-Vehn, *The Physics of Inertial Fusion*, Oxford University, Oxford (2004).
- [5] D. H. Munro *et al.*, Phys. Plasmas 8, 2245 (2001).
- [6] R. L. McCrory *et al.*, Nucl. Fusion 41, 1413 (2001).
- [7] R. Betti *et al.*, Phys. Rev. Lett. 98, 155001 (2007).
- [8] D. O. Gericke, M. S. Murillo, and M. Schlenges, Phys. Rev. E 65, 036418 (2002).
- [9] L. S. Brown, D. L. Preston and R. L. Singleton, Jr, Phys. Rep. 410, 237 (2005).
- [10] L. S. Brown and R. L. Singleton, Jr, Phys. Rev. E 76, 066404 (2007).
- [11] M. S. Murillo and M.W.C. Dharma-wardana, Phys. Rev. Lett. 100, 205005 (2008).
- [12] B. Jeon *et al.*, Phys. Rev. E 78, 036403 (2008).
- [13] G. Dimonte and J. Daligault, Phys. Rev. Lett. 101, 135001 (2008).
- [14] L. D. Landau, Phys. Z. Sowjetunion, 10 (1936) 154.
- [15] L. Spitzer, *Physics of Fully Ionized Gases*, Wiley, New York (1962).
- [16] P. Celliers *et al.*, Phys. Rev. Lett. 68, 2305 (1992).
- [17] A. Ng *et al.*, Phys. Rev. E 52 4299 (1995).
- [18] J. M. Laming *et al.*, Astrophysical Journal, 472, 267 (1996).
- [19] J. M. Taccetti *et al.*, J. Phys. A 39, 4347 (2006).
- [20] J. J. Garet *et al.*, High Energy Density Phys. 2, 83 (2006).
- [21] R. D. Petrasso *et al.*, Phys. Rev. Lett. 90, 095002 (2003).
- [22] J. A. Frenje *et al.*, Phys. Plasmas 11, 2798 (2004).
- [23] J. R. Rygg *et al.*, Phys. Plasmas 15, 034505 (2008).
- [24] T. R. Boehly *et al.*, Opt. Commun. 133, 495 (1997).
- [25] S. Skupsky *et al.*, Phys. Plasmas 6, 2157 (1999).
- [26] H.-S. Bosch and G. M. Hale, Nucl. Fusion 32, 611 (1992).
- [27] R. A. Lerche *et al.*, Rev. Sci. Instrum. 66, 933 (1995).
- [28] F. H. Séguin *et al.*, Rev. Sci. Instrum. 74, 975 (2003).
- [29] Protons from the shell material are accelerated by electrostatic fields while the laser pulse illuminates the capsule. These fields have decayed well before the time of nuclear production, several 100 ps after the end of the pulse, so do not affect nuclear product spectra. See also D. G. Hicks *et al.*, Phys. Plasmas 8, 606 (2001).
- [30] J. R. Rygg, Ph.D. Thesis, Massachusetts Institute of Technology (2006), Appendix C.
- [31] Note that the "shock-burn-averages" discussed in this article are not direct spatio-temporal averages, but are weighted by the DD-p and D<sup>3</sup>He nuclear production rates, which have strong temperature and density dependence.
- [32] C. K. Li *et al.*, Phys. Plasmas 7, 2578 (2000).
- [33] C. K. Li and R. D. Petrasso, Phys. Rev. Lett. 70, 3059 (1993).
- [34] J. H. Gardner *et al.*, J. Fluid Mech. 114, 41 (1982).
- [35] J. R. Rygg *et al.*, Phys. Rev. Lett. 98, 215002 (2007).
- [36] R. P. Drake, *High Energy Density Physics*, Springer, New York (2006).
- [37] Note that the parameter  $\tau_{ei}$  – commonly called the electron-ion equilibration time constant – is not actually constant in time for the large temperature differences considered here.
- [38] The large ion-electron mass ratio makes collisions inefficient for exchanging energy between the two species, so generally the individual species will equilibrate on a much faster time scale than the relaxation between the species.

- [39] The 12.7 keV root gives  $T_f = 5.1$  keV, and a characteristic time of 1270 (3660) ps. At peak shock-burn, the corresponding ion temperature would be 8.8 (10.4) keV.
- [40] More appropriate to describe the overall shape of the relaxation curve is  $\tau_f$ , the equilibration time constant at the equilibrium temperature described in Eq. (12):  $\tau_f = 880$  (3900) ps for high (low)  $\rho_0$ . However, since  $\Delta t_s \ll \tau_f$ ,  $\tau_f$  is not suitable for describing the coupling time characteristic of the plasma during shock burn.